

Suppressing Nanoparticle-Mononuclear Phagocyte System Interactions of Two-Dimensional Gold Nanorings for Improved Tumor Accumulation and Photothermal Ablation of Tumors

Yijing Liu,^{†,∇} Zhantong Wang,^{†,∇} Yi Liu,^{‡,§} Guizhi Zhu,[†] Orit Jacobson,[†] Xiao Fu,[†] Ruiliang Bai,^{||} Xiaoying Lin,[‡] Nan Lu,[†] Xiangyu Yang,[†] Wenpei Fan,[†] Jibin Song,^{†,||} Zhe Wang,[†] Guocan Yu,[†] Fuwu Zhang,[†] Heather Kalish,[⊥] Gang Niu,[†] Zhihong Nie,^{*,‡,||} and Xiaoyuan Chen^{*,†,||}

[†]Laboratory of Molecular Imaging and Nanomedicine and [⊥]Trans-NIH Shared Resource on Biomedical Engineering and Physical Science, Institute of Biomedical Imaging and Bioengineering and ^{||}Section on Quantitative Imaging and Tissue Science, Division of Imaging, Behavior, and Genomic Integrity, Eunice Kennedy Shriver National Institute of Child Health and Human Development, National Institutes of Health, Bethesda, Maryland 20892, United States

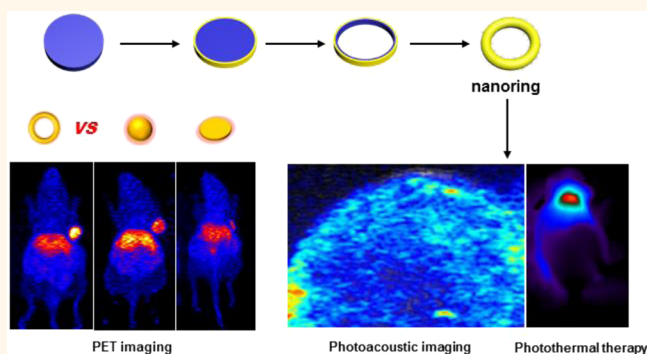
[‡]Department of Chemistry and Biochemistry, University of Maryland, College Park, Maryland 20742, United States

[§]State Key Laboratory of Supramolecular Structure and Materials, College of Chemistry, Jilin University, Changchun 130012, P. R. China

Supporting Information

ABSTRACT: The clearance of nanoparticles (NPs) by mononuclear phagocyte system (MPS) from blood leads to high liver and spleen uptake and negatively impacts their tumor delivery efficiency. Here we systematically evaluated the *in vitro* and *in vivo* nanobio interactions of a two-dimensional (2D) model, gold (Au) nanorings, which were compared with Au nanospheres and Au nanoplates of similar size. Among different shapes, Au nanorings achieved the lowest MPS uptake and highest tumor accumulation. Among different sizes, 50 nm Au nanorings showed the highest tumor delivery efficiency. In addition, we demonstrated the potential use of Au nanorings in photoacoustic imaging and photothermal therapy. Thus, engineering the shape, surface area, and size of Au nanostructures is important in controlling NP–MPS interactions and improving the tumor uptake efficiency.

KEYWORDS: gold nanorings, nanobio interactions, macrophage uptake, tumor accumulation, photoacoustic imaging, photothermal therapy



The evolving nanotechnology over the past few decades has generated nanoparticles (NPs) with sophisticated shapes and fine-tuned sizes, accelerating the research on nanomedicine for cancer therapy. The shape- and size-dependent physicochemical properties of NPs are promising to improve the diagnostic and therapeutic outcomes of nanomedicine.^{1–3} Compared to conventional small molecule medicine, NPs are expected to show preferential and increased accumulation in tumors through the so-called enhanced permeability and retention (EPR) effect.^{4,5} More recently, researchers found that NPs could induce endothelial cell barrier

leakiness (NanoEL effect) to further enhance the drug delivery efficiency.^{6,7} Despite the EPR effect and the NanoEL effect, NPs would encounter a series of biological barriers immediately after systemic administration, which dramatically impede their tumor delivery efficiency.^{8,9} One of the biggest obstacles for the intravenously administered NPs is their rapid clearance from blood circulation by cells of the mononuclear phagocyte system

Received: August 18, 2017

Accepted: September 27, 2017

Published: September 27, 2017

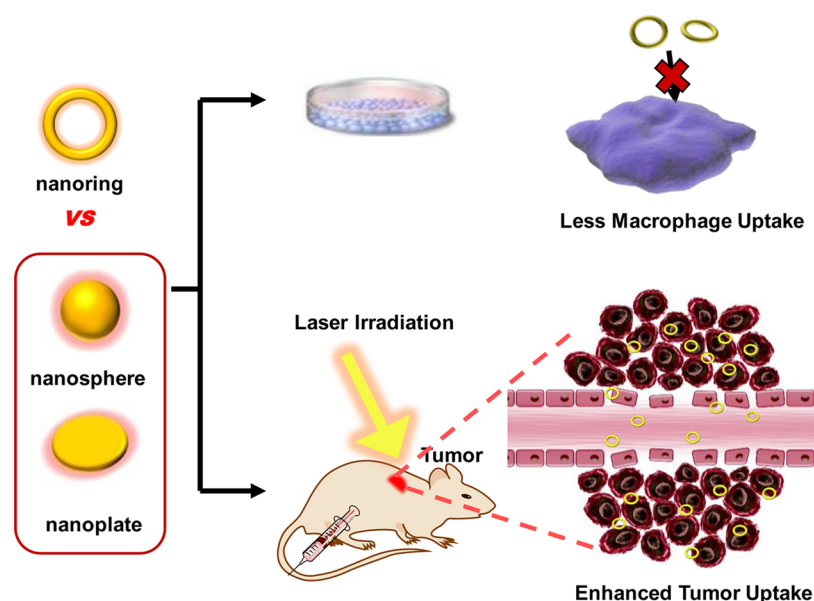


Figure 1. Schematic illustration of shape effect on NP–MPS interactions and tumor accumulation of Au nanorings compared with Au nanospheres and Au nanoplates. Au nanorings showed the lowest uptake by macrophage cells *in vitro* and highest tumor uptake *in vivo*.

(MPS) and undesired accumulation in organs like liver and spleen, severely limiting the percentage of NPs reaching target site.¹⁰ The inability of NPs to overcome these biological barriers reflects our insufficient understanding and control over the interactions between NPs and biological system (*i.e.*, nanobio interactions), such as formation of protein corona, NP–cell interactions, NP–MPS interactions, and tumor uptake.^{10–13}

Among different nanomaterials, gold NPs (Au NPs) represent excellent models to study the shape and size effects on nanobio interactions, due to their narrow size distributions, excellent stability, and great potentials in biomedical applications resulting from their tunable optical properties and photothermal effects.^{1,14–18} For *in vivo* biomedical applications, such as photothermal agents for cancer therapy or photoacoustic (PA) imaging contrast agents, Au NPs with absorption in the near-infrared (NIR) range are preferred.^{14,19,20} The geometric parameters of Au NPs, including shape and size, have been reported to greatly impact both their optical properties and nanobio interactions.^{1–3,18,21–23} Various Au nanostructures with NIR absorption, including Au nanorods, Au nanocages, and Au nanoshells, have been prepared.^{15,24,25} In addition, recent studies have shown that nonspherical nanostructures, such as disk-like and elongated NPs, may target tumors more efficiently than spherical NPs by reducing the NP–MPS interactions and increasing the NPs' propensity of margination in blood vessels.^{26–31} However, previous studies of shape effect on nanobio interactions usually use AuNPs with distinct surface chemistry or sizes, which add other variables in addition to shape effect, leading to several possible explanations for experimental phenomena or ambiguous results.^{18,23} For example, the use of cetyltrimethylammonium bromide (CTAB) containing AuNPs, such as Au nanorods, would cause stronger nonspecific interactions between positively charged AuNPs and negatively charged cell membranes than using negatively charged AuNPs.

The Au nanoring, with two-dimensional (2D) and hollow features, is one type of nonspherical nanostructure with NIR absorption, of which the nanobio interactions have not been

adequately explored.^{32,33} Compared to spherical or cylindrical NPs, the use of 2D Au nanomaterials, like Au nanorings or Au nanoplates, in the study of nanobio interactions, allows us to control the contact area between NPs and cells without changing the size of NPs and obtain more straightforward correlations between NP shapes and nanobio interactions.

We report here a systematic study of the shape and size effect of a model of 2D nanomaterials, Au nanorings, on nanobio interactions by evaluating their macrophage uptake, biodistribution in different organs, such as liver and spleen, and tumor uptake. All the Au nanostructures were initially stabilized by sodium citrate, which were further replaced by thiol-terminated poly(ethylene glycol) methyl ether (M_w 5000 g/mol) (HS-PEG). To understand the shape effect of Au nanorings, the macrophage uptake and biodistribution of Au nanospheres and Au nanoplates of similar size were also studied (Figure 1). We found that 50 nm Au nanorings had the lowest percentage of uptake by macrophages, followed by Au nanospheres and Au nanoplates of similar size *in vitro*. The preformed protein corona on the surfaces of Au NPs would decrease the cell uptake of all three types of Au nanostructures, yet the uptake of Au nanorings remains to be the lowest. The *in vivo* data showed that 50 nm Au nanorings had a lower total uptake in the liver and spleen and higher tumor accumulation than NPs with other shapes. Our hypothesis is that the smaller contact area between Au nanorings and cell and 2D shape accounts for the overall lower cell uptake compared to other Au nanostructures. In addition, depending on the initial contact angle between NPs and cells, the high local curvature at the edges of 2D nanostructures may also influence the endocytosis process.^{34,35} Furthermore, we examined a series of Au nanorings between 25 and 130 nm to determine the best size for tumor delivery. Among different sizes, 50 nm Au nanorings accumulated higher in tumors than both 25 and 130 nm Au nanorings at 48 h after systemic administration. However, 25 nm Au nanorings accumulated more rapidly in tumors at early time points, which can be explained by the size differences of transient and static openings at leaky blood vessels or the NanoEL effect.^{4,6} Finally, we demonstrated the potential

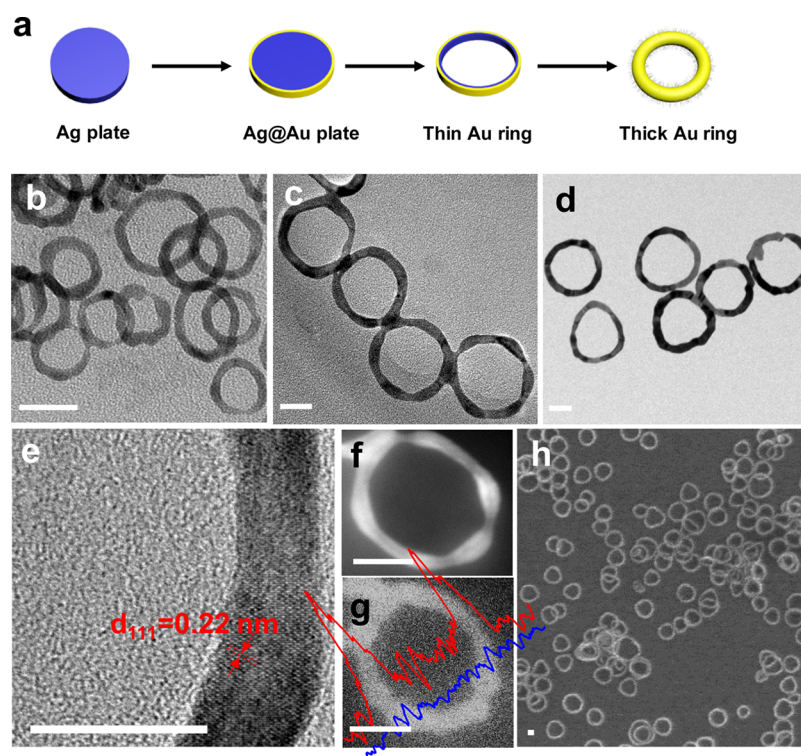


Figure 2. The schematic illustration of the synthesis of Au nanorings and the TEM and SEM characterizations of Au nanorings. (a) Schematic illustration of the synthesis of Au nanoring. (b–d) Representative TEM images of Au nanorings with diameter of (b) 25 nm, (c) 50 nm, and (d) 130 nm. (e) High-resolution TEM image of Au nanoring. (f) High-annular dark-field TEM image and (g) energy dispersive X-ray spectroscopy characterization of Au nanoring. (h) SEM image of Au nanorings. Scale bars: 20 nm.

applications of Au nanorings as PA imaging contrast agents and photothermal therapeutics. The results from this study indicate that suppression of NP–MPS interactions and improvement of *in vivo* delivery efficiency can be achieved by accurate engineering of the shape, surface area, and size of nanomaterials and will identify important design rules for the development of next-generation of nanomedicine.

RESULTS AND DISCUSSION

Synthesis of Au Nanorings. Au nanorings were fabricated through a template method by selective Au deposition on the edges of silver (Ag) nanoplates and subsequent Ag etching, followed by a second Au deposition (Figure 2a and Figure S1a–c). The Ag nanoplate templates had an absorption peak of 628 nm. The coating of Au on the edges of Ag nanoplates led to a red-shift of absorption peak to 700 nm (Figure S1d). After removing the Ag templates, the appearance of broad absorption from 570 nm to near-infrared (NIR) range indicated the formation of thin Au nanorings (Figure S1d). The initial stabilizing ligand on Au nanorings was sodium citrate, which was subsequently replaced by HS-PEG (M_w 5000 g/mol) through a ligand exchange reaction. Different sized Au nanorings were synthesized by tuning the sizes of Ag nanoplate templates, which can be readily adjusted by controlling the ratio between Ag seeds and growth solution (see Methods for experimental details). Au nanorings with three different sizes were used in the present study, of which the average largest dimensions were 25, 50, and 130 nm, determined by both transmission electron microscopy (TEM) observations and dynamic light scattering (DLS) measurements (Figure 2b–d and Figure S2). The lattice spacing of Au nanorings after second Au deposition under high-resolution TEM was around

0.22 nm, corresponding to Au (111) fcc planes (Figure 2e). High-angle annular dark-field-scanning TEM-energy dispersive X-ray spectroscopy (HAADF-STEM-EDS) image (Figure 2f,g) and inductively coupled plasma optical emission spectroscopy (ICP-OES) confirmed that nanorings are composed of 90 wt% Au. The SEM image shows the large area uniformity of Au nanorings (Figure 2h).

The optical and photothermal properties of Au nanorings are related to their thicknesses, which can be readily adjusted through controlling the second Au deposition time (Figures S3 and S4a). The initial Au nanorings after etching had a thickness of 2 nm and exhibited a weak UV–vis absorption before 500 nm and a strong NIR absorption after 570 nm (Figure S1d). When the ring thickness was increased from 2 to 20 nm, a red-shift of UV–vis absorption peak to 508 nm and a blue-shift of NIR absorption peak to 778 nm occurred simultaneously (Figure S4b). The thickness-dependent absorption feature can be explained by the symmetry mode of electro-magnetic coupling between the inner and outer ring walls.³⁶ Then, we investigated how the thickness of Au nanoring affects the photothermal properties. We monitored the temperature changes of solutions of Au nanorings of different thicknesses with the same Au concentration under NIR laser irradiation (808 nm 0.5 W/cm²). The maximum temperature change and the calculated photothermal conversion efficiency were found to decrease with increasing ring thickness, which can be explained by the larger fraction of light scattering of thicker Au nanorings (Figure S4c–e).³⁷ The calculated photothermal conversion efficiency of Au nanorings with thicknesses of 4, 9, and 20 nm were 43.5 ± 3.2 , 37.9 ± 2.2 , and $31.9 \pm 2.3\%$, respectively. In addition to photothermal conversion efficiency, we found that thicker Au nanorings showed better photo-

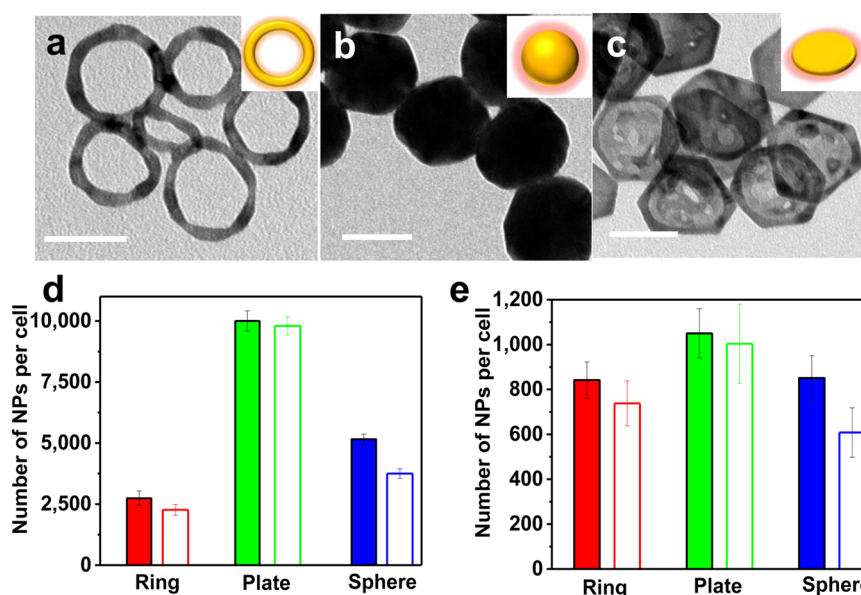


Figure 3. Study of shape effect of Au nanorings on macrophage uptake *in vitro* compared to Au nanospheres and Au nanoplates. (a–c) Representative TEM images of (a) Au nanorings, (b) Au nanospheres, (c) and Au nanoplates. Scale bars: 50 nm. (d–e) Columns show shape-dependent raw 264.7 cell uptake of Au nanorings, Au nanoplates, and Au nanospheres at 37 °C for 8 h (d) and 4 °C for 1 h (e) without (filled columns) and with (hollow columns) preformed protein corona (mean \pm s.d.; $n = 3$).

thermal stability than thinner ones (Figure S5). Taking both photothermal conversion efficiency and photothermal stability into account, we chose 50 nm Au nanorings with 9 nm thickness to study their shape effect on nanobio interactions.

Cytotoxicity Assay and Stability of Au Nanorings.

First, we analyzed the cell viability after their incubation in the presence of each type of Au nanostructure, including Au nanorings, Au nanoplates, and Au nanospheres (Figure 3a–c and Figure S6). Au NPs with size around 50 nm were chosen because previous reports indicated that this is the optimized size for tumor delivery of Au spheres.³⁸ Similar to Au nanorings, the ligands on Au nanospheres and Au nanoplates were changed from sodium citrate to HS-PEG. Raw 264.7 cells were treated with three Au nanostructures with different concentrations of Au for 24 h in Dulbecco Minimum Essential Medium (DMEM) plus 10% serum. The results from MTT assay showed that the cell viability after their incubation with the three Au nanostructures was above 88% even at a high concentration (150 $\mu\text{g}/\text{mL}$) of Au, which indicated very low cytotoxicity of Au NPs used in our current study (Figure S7). Then, we studied the stability of Au nanostructures in biological medium. All three Au nanostructures were incubated with DMEM plus 10% serum, and DLS and TEM images were checked before and 48 h after the incubation. DLS results indicated that there was no significant size change of Au NPs after 48 h incubation with DMEM with 10% serum (Table S1). The stability of Au nanostructures was also confirmed by TEM images and absorption spectra (Figures S8 and S9).

Shape Effect of Au Nanorings on Macrophage Uptake *in Vitro*. We investigated the effect of shape on the uptake level of three different Au nanostructures by macrophage-like Raw 264.7 cells *in vitro*. First, we incubated Raw 264.7 cells with equal molar concentrations of Au nanorings, Au nanospheres, and Au nanoplates with diameters around 50 nm for 8 h in DMEM plus 10% serum. After incubation, we detached cells from Petri dish, digested the cells with aqua regia, and measured the concentrations of Au by ICP-OES, which were

converted into number of AuNPs per cell (see Supplementary Methods for experimental details). Among different structures, the uptake level of Au nanorings by Raw 264.7 cells was the lowest, followed by Au nanospheres and Au nanoplates (Figure 3d).

The cell uptake of NPs is presumably through receptor-mediated endocytosis, derived from nonspecific adsorption of serum proteins on NPs with incomplete PEGylation.^{13,39} During endocytosis, receptors on the cell membrane will diffuse toward NP binding sites to interact with the NP, and the cell membrane will deform and wrap around NPs to internalize the NP.⁴⁰ The shape of NPs would affect their contact area toward cells and therefore the adhesion between NPs and cells.^{41,42} The flat surface of 2D Au nanoplates provides a larger contact area with the cell membrane, leading to stronger adhesion toward cells, which partially explains their higher uptake by cells (Figure 3d). While Au nanorings are also a type of 2D nanomaterial, the central hole in the ring structure reduces the contact area between NPs and the cell membrane, leading to their lower level of cell uptake compared to Au nanoplates. Similarly, the cell uptake of Au nanospheres, with relatively high surface curvature, is lower than that of Au nanoplates because of the smaller contact area with the cell membrane. To characterize the adhesion between different NPs and the cell membrane, we incubated the cells with NPs at 4 °C for 1 h and measured the number of NPs attached on the cell membrane by ICP-OES. The incubation at low temperature would inhibit the active internalization process, isolating the NPs adhered on the cell membrane from the rest of endocytosis process.⁴² We found that the number of Au nanoplates attached to the cell membrane was higher than that of Au nanospheres and Au nanorings (Figure 3e), which indicated the stronger adhesion between Au nanoplates and the cell membrane. The cell uptake of Au nanorings is lower than Au nanospheres. It is possible that the 2D shape of NPs may also affect the rotation of NPs in the cell membrane or the specific endocytosis pathway and therefore the uptake level of

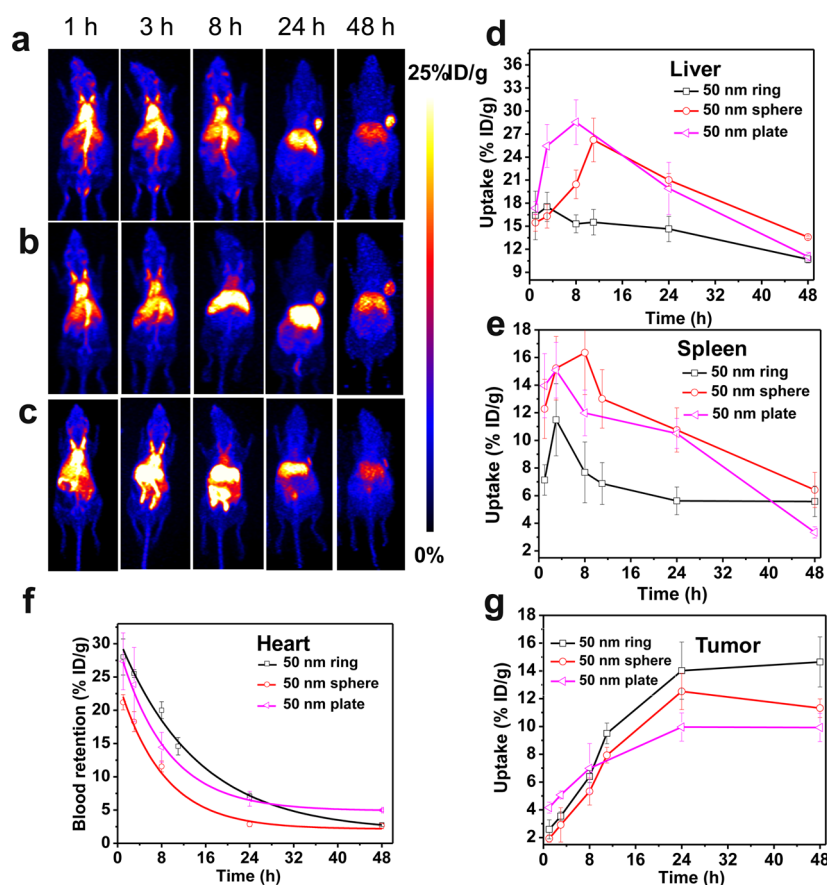


Figure 4. Study of Au nanorings shape effect on *in vivo* biodistribution and tumor accumulation compared to Au nanospheres and Au nanoplates. (a–c) Representative whole-body coronal PET images of mice after intravenous injection of ^{64}Cu -labeled (a) Au nanorings, (b) Au nanospheres, and (c) Au nanoplates. (d–g) Time activity curves of the mean uptake of ^{64}Cu -labeled Au nanostructures in (d) liver, (e) spleen, (f) tumor, and (g) blood derived from the region of interest (ROI) analysis of the PET images (mean \pm s.d.; $n = 3/\text{group}$).

NPs during endocytosis.⁴³ Besides the different contact area, the high curvature at the edges of Au nanoplates or Au nanorings may also influence their uptake by macrophage cells. The detailed mechanism needs further investigation.

To better mimic the adsorption of serum proteins on NP surfaces in biological milieu, all NPs were treated with 100% human serum for 2 h before incubation with cells. To confirm the adsorption of serum proteins, we extracted the proteins from the surfaces of Au NPs and studied the compositions of the protein layer using polyacrylamide gel electrophoresis (PAGE) with fluorescence staining (Figure S10). The complex band patterns indicated that a broad range of proteins were adsorbed on the surfaces of Au NPs. The DLS and zeta potential were also used to characterize the Au NPs without and with the adsorption of serum proteins (Table S2). After incubating the cells with three Au nanostructures with preformed protein corona, the uptake level of different Au nanostructures was analyzed. The order of the cell uptake level is similar to Au NPs without preformed protein corona, even though a slightly decreased cell uptake level was observed for all three Au nanostructures. This result indicated that the formation of protein corona on NPs negatively impacted their uptake by cells of Au NPs, yet the effect of NP shape on cell uptake was preserved. Similarly, a decreased level of cell adhesion of NPs with preformed protein corona was observed for all different nanostructures. The result indicated that the decreased uptake of NPs with preformed protein corona by cells could be caused by the reduced adhesion between NPs

and the cell membrane, possibly through reducing the nonspecific interactions between NPs and cells.

***In Vivo* Shape Effect of Au Nanorings on Liver Uptake and Tumor Accumulation.** We then investigated shape effects of Au structures on MPS-NP interactions *in vivo* by using female nude mice bearing subcutaneous U87MG tumors on the flank as a model. The Au nanostructures were labeled with ^{64}Cu radioisotope, and their biodistribution in different organs, such as liver, spleen, heart, and tumor was monitored through PET imaging (see Supplementary Methods for experimental details). Radionuclide-based PET imaging is a noninvasive imaging technique with high sensitivity and the ability to conduct quantitative analysis of whole-body images (Figure 4a–c).⁴⁴ It allows real-time pharmacokinetics monitoring of radioisotope-labeled nanomedicine. First, we analyzed the accumulation of different Au nanostructures in the liver. We found that Au nanoplates had the highest liver uptake, followed by Au nanospheres and Au nanorings (Figure 4d). Specifically, the percent injected dose per gram tissue (%ID/g) of Au nanoplates accumulated in the liver was the highest at 8 h after administration ($28.5 \pm 2.9\% \text{ID/g}$), which was higher than that for Au nanospheres ($20.4 \pm 1.9\% \text{ID/g}$) and Au nanorings ($15.3 \pm 1.2\% \text{ID/g}$) at the same time point. For Au nanospheres, the highest liver uptake ($26.2 \pm 2.8\% \text{ID/g}$) was reached at 11 h after administration. A relatively lower extent of Au nanorings were in the liver at all time points, of which the area under the curve (AUC) for liver uptake was 27.7% and 29.4% lower than Au nanospheres and Au nanoplates, respectively. Like what we

observed in the liver, Au nanorings showed the lowest spleen uptake among three different Au nanostructures of similar size (Figure 4e). Yet, the spleen sequestered less Au NPs per gram of tissue than the liver in all three cases, and the AUC for the spleen uptake of Au nanospheres was slightly higher than that of Au nanoplates. The differences between spleen and liver on NP uptake may come from the different phenotypes of macrophage cells and the disparity of cardiac output received in the above two organs.¹⁰ The macrophage cells in the liver show stronger endocytic affinity to hard nanomaterials than macrophages in the spleen, and the liver receives more than 20 times higher cardiac output than spleen.¹⁰

Furthermore, we measured the concentrations of Au in blood (%ID/g) as a function of time by quantifying the ⁶⁴Cu signal at left ventricles for all three different Au nanostructures (Figure 4f). The fast clearance of NPs from blood through NP–MPS interaction is expected to shorten their blood circulation half-lives. Indeed, the circulation half-life of 50 nm Au nanorings ($t_{1/2} = 9.8$ h) was longer than that of Au nanospheres ($t_{1/2} = 5.6$ h) and Au nanoplates ($t_{1/2} = 6.0$ h).

To achieve tumor targeting, NPs have to cross the blood-tumor barrier through both static pores and dynamic vents, which would be favored for NPs with long blood retention.⁴ This agrees with our observations as the accumulation of Au nanorings in tumors was higher than Au nanospheres and Au nanoplates, increasing from $2.6 \pm 0.7\%$ ID/g at 1 h to $14.0 \pm 2.1\%$ ID/g at 24 h and up to $14.6 \pm 1.8\%$ ID/g at 48 h after administration (Figure 4g). The accumulation of Au nanospheres and nanoplates in tumors at 48 h was $11.3 \pm 0.7\%$ ID/g and $9.9 \pm 1.0\%$ ID/g, respectively (Figure 4g). The maximum tumor accumulation of Au nanospheres occurred at 24 h after injection, while the accumulation of Au nanorings and Au nanoplates was the highest at 48 h after injection. The retention of Au NPs in tumors is related to the blood retention of NPs because NPs can both enter and exit the tumors and the directions of diffusion depend on the relative concentration of NPs between blood and tumor tissue. Therefore, the Au nanospheres with shortest blood circulation half-life reached the maximum tumor uptake earlier than Au nanorings and Au nanoplates. At 48 h postinjection, the mice were sacrificed, and the major organs were harvested and weighed for *ex vivo* biodistribution study by measuring the signal of ⁶⁴Cu in different organs under a gamma counter. The results of *ex vivo* study were in accordance with those measured from PET imaging (Figure S11).

We used PET images to analyze the distributions of Au nanostructures within tumors. PET data can provide 3D information on tumor tissues by showing the images of slices of tumor tissue cross sections. We checked the PET images of tumor cross sections at 24 h after injection of different AuNPs. PET signals of Au nanorings and Au nanoplates were distributed in the entire tumor tissues, but with stronger PET signals of Au nanospheres located at the periphery of tumor tissues (Figure S12). The results suggested a better distribution of ring or plate structure over sphere structure in tumor tissues. Compared to the Au nanosphere, the Au nanoring is hollow in the center and is smaller in size in one dimension, which would show better diffusive properties and encounter smaller resistance than Au nanospheres in tumor tissue. We used a simplified mathematical model to calculate diffusivity of the different Au nanostructures following the Stokes–Einstein equation by considering the movement of Au nanoparticles in

tumor tissues as random walks (see Supplementary Methods for details of calculations):^{45,46}

$$D = \frac{k_B T}{\zeta}$$

where k_B , T , and ζ represent Boltzmann's constant, temperature, and Stoke's drag coefficient, respectively. The diffusivity of the Au nanoring is 50% higher than the Au nanosphere. The diffusivities of the Au plate and Au nanoring are very close. Therefore, a more uniform distribution of Au nanoplates and Au nanorings in tumor tissues were observed. The consistency between experimental observation and mathematical calculation suggests the advantage of Au nanoring over other structures in tumor delivery.

Size Effect of Au Nanorings on Liver Uptake and Tumor Accumulation. In addition to NP shape, it has been reported that NP size plays an important role in affecting particle distribution *in vivo*.^{3,21} Therefore, we prepared Au nanorings with diameters of 25, 50, and 130 nm and systematically explored the size effect of Au nanorings on the *in vivo* biodistribution to determine the best size for tumor delivery. The thicknesses of both 50 and 130 nm Au nanorings were around 9 nm. The thickness of 25 nm Au nanorings was set to 4 nm to strengthen the hollow feature of ring structure. PET data were used to analyze the biodistribution of Au nanorings with different sizes after intravenous injection (Figures S13 and S14). For 25 nm Au nanorings, a relatively low accumulation in the liver and spleen was observed (Figures S13 and 14a,b). The circulation half-life of 25 nm Au nanorings was about 5.6 h (Figure S14c). In terms of tumor targeting, 25 nm Au nanorings had a significant accumulation of $13.6 \pm 1.6\%$ ID/g 24 h after the injection, which was only slightly less than that of 50 nm rings (Figure S14d). Besides the relatively high tumor accumulation, 25 nm Au nanorings showed a faster tumor uptake rate than 50 nm rings at early time points. As a comparison, the accumulation of 25 nm Au nanorings in tumors increased from $3.6 \pm 0.3\%$ ID/g at 1 h to $8.4 \pm 1.3\%$ ID/g at 8 h, while during the same period the accumulation of 50 nm Au nanorings only increased from $2.6 \pm 0.7\%$ ID/g to $6.4 \pm 0.4\%$ ID/g (Figure S14d). However, at late time points, 50 nm Au nanorings surpassed 25 nm Au nanorings in tumor accumulation. On the one hand, NPs with a smaller size are superior to their larger counterparts in crossing the blood vessel barriers as there is a size limitation on the static permeability of vessel walls.⁴ It is also possible that the better permeability of smaller-sized NPs was due to their stronger NanoEL effect.^{47,48} On the other hand, smaller sized NPs are also easier to diffuse back from tumor tissues to blood vessels. When 130 nm Au nanorings were injected, their rapid clearance from blood by phagocytic cells of the MPS was observed, leading to high liver and spleen accumulations at 1 h after the injection (Figure S14 a,b). As a result, 130 nm Au nanorings showed a short blood circulation half-life of 0.1 h and poor tumor accumulation (Figure S14 c,d). The *in vivo* PET observations were confirmed by the *ex vivo* biodistribution study (Figure S15).

Au Nanorings for PA Imaging and Photothermal Therapy. Au nanorings with strong NIR absorption and high tumor delivery efficiency have great potentials in various biomedical applications.^{32,33} Here we demonstrated the potential biomedical applications of 50 nm Au nanorings as PA contrast agents and photothermal therapeutic agents *in vivo*. PA imaging can visualize the tumors or organs with enhanced

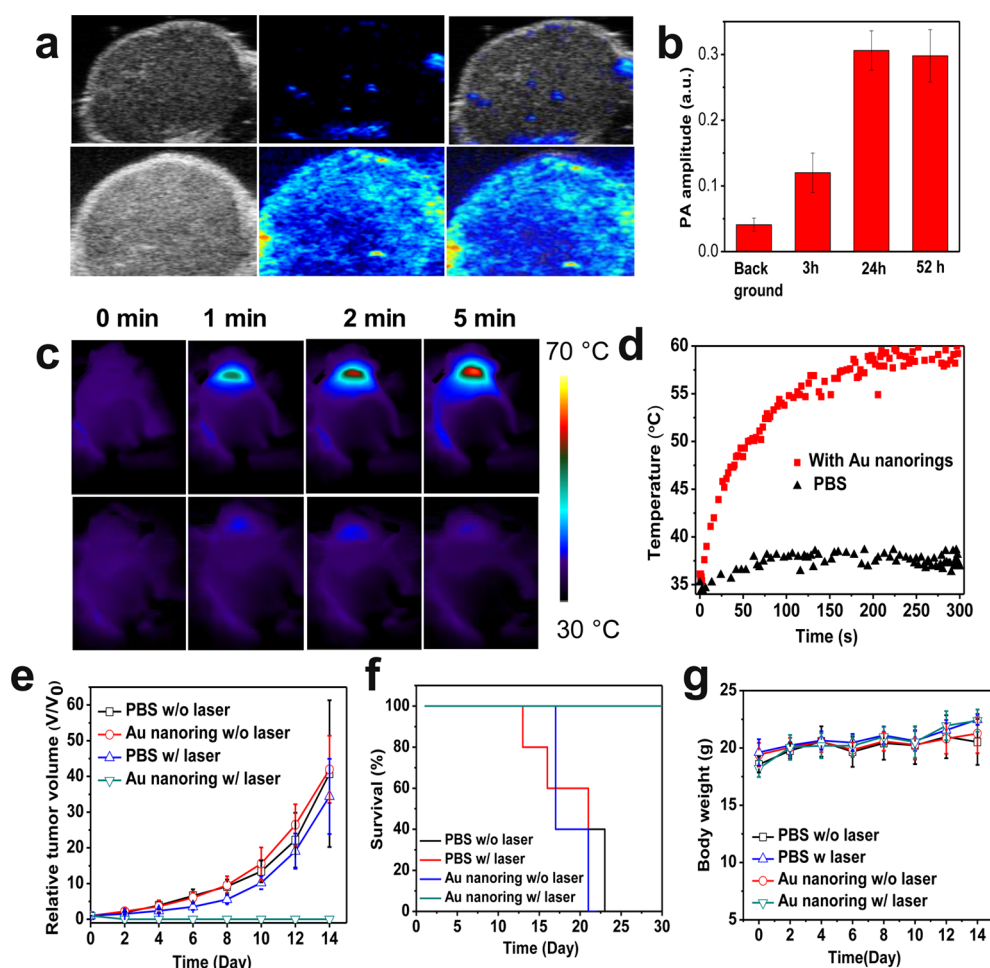


Figure 5. Au nanorings as PA contrast agent and photothermal therapeutics. (a) Ultrasonic (US), PA images, and merged images of tumors (from left to right) before (upper row) and 24 h after (lower row) intravenous injection of Au nanorings. (b) PA intensities of tumor tissues before and at 3, 24, and 52 h after injection. (c) Thermal images of U87MG tumor mice injected intravenously with 50 nm Au nanorings (upper) and PBS (lower) upon 5 min laser irradiation and (d) corresponding temperature change of tumor area. (e) Relative tumor volume, (f) survival curves, and (g) body weight curves of treatment group and all other control groups ($n = 3/\text{group}$).

imaging depth and higher spatial resolution than typical fluorescence imaging techniques.¹⁷ PEGylated 50 nm Au nanorings were intravenously injected into U87MG tumor-bearing nude mice, followed by irradiation of tumor tissues with an 808 nm pulsed laser at different time points postinjection. Compared to the background signal, a 7.7 times signal enhancement was obtained 24 h after injection of Au nanorings (Figure 5a,b). The strong signal enhancement suggested high accumulation of Au nanorings in tumors. We then applied the Au nanorings as a photothermal therapeutic agent using the same animal model. Based on the PET results, we conducted the photothermal treatment at 48 h after the injection by irradiating the tumor area with 808 nm continuous-wave laser for 5 min ($0.75 \text{ W}/\text{cm}^2$). A significant temperature increase in the tumor tissues compared to the PBS group was observed (Figure 5c,d). After irradiation, tumor volumes and mice weight of all groups were recorded every 2 days in the entire experiment. Remarkably, in the experiment group with injections of Au nanorings, all the tumors were completely eliminated, and an improved survival rate was achieved (Figure 5e, f). Fast tumor growth was observed in all other control groups, which included intravenous injection of PBS with or without laser irradiation and injection of Au nanorings without laser irradiation (Figure 5e).

During the experiment, no apparent weight loss was observed in the control group, in which Au nanorings were injected without laser irradiation, indicating the low toxicity of Au nanorings (Figure 5g). The *in vivo* toxicity and therapeutic effect of Au nanorings were also evaluated through hematoxylin and eosin (H&E) staining of primary organs and tumors. Major organs of mice from control group and experimental group were collected 15 days after treatment, and no obvious sign of toxic effects from Au nanorings were observed through H&E staining (Figure 6a,b). This result suggested the low toxicity of Au nanorings. In addition, the H&E-stained images of tumor sections collected 4 h after the treatment showed serious damage of cancer cells compared to the control group (Figure 6c,d). This result demonstrated the excellent therapeutic effect of Au nanorings.

CONCLUSION

We have systematically evaluated the effect of shape of 2D Au nanorings on nanobio interactions both *in vitro* and *in vivo* by comparing with Au nanospheres and Au nanoplates of similar size. *In vitro* experiments demonstrated that Au nanorings with a diameter of 50 nm can greatly decrease the uptake of NPs by macrophage cells compared to Au nanoplates and Au nanospheres of similar size. The difference in macrophage

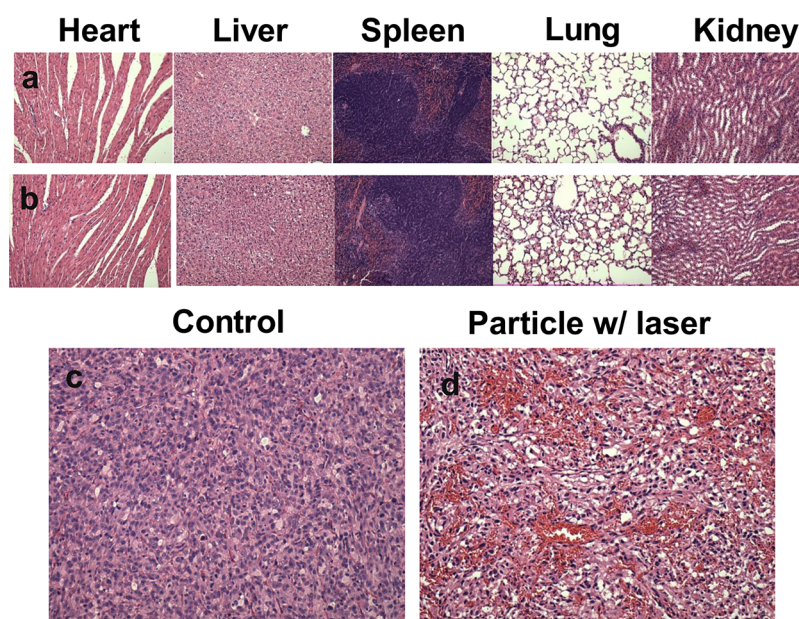


Figure 6. H&E staining of primary organs and tumor tissues without or with photothermal treatment. H&E staining of major organs 15 days after the treatment with the injection of (a) PBS and (b) Au nanorings. H&E staining of tumor tissues (c) without or (d) with photothermal treatment.

uptake was due to the unequal contact areas between NPs and cells, which influences the adhesion between them. Among different structures, Au nanoplates with the largest contact area between Au nanostructures and cells showed the highest uptake by macrophages. The 2D ring structure showed the lowest uptake by macrophage cells. Besides distinct surface areas, the high curvature at the edges of 2D nanostructures may also play a role in influencing the macrophage uptake. The formation of protein corona on NP surfaces decreased the uptake level of all three types of NPs by macrophage cells. The *in vivo* data indicated that 50 nm Au nanorings showed lower accumulation in livers or spleens and higher accumulation in tumors than Au nanospheres and Au nanoplates. Therefore, the lower MPS clearance of Au nanostructures *in vivo* can only be achieved by choosing NPs with proper shape. Furthermore, we evaluated the size effect of Au nanorings on tumor delivery. Among 25, 50, and 130 nm Au nanorings, 50 nm Au nanorings showed the highest tumor delivery efficiency, but 25 nm Au nanorings accumulated in tumors faster than 50 nm Au nanorings at early time points postinjection with an overall modest tumor delivery efficiency. Finally, we demonstrated the imaging and therapeutic functions of Au nanorings in an animal model. These findings indicate that engineering the shape and surface area of Au nanostructures is very important in mediating NP–MPS interactions and tumor delivery efficiency and will lay the ground for rational designs of nanomedicine for biomedical applications in the future.

METHODS

Preparation of Ag Nanoplates. Ag nanoplates were prepared according to previous literature with some modification.⁴⁹ First, Ag seeds were prepared as follows: To 200 mL of water, aqueous solutions of sodium citrate (0.0045 M), silver nitrate (1×10^{-4} M), and 480 μ L H_2O_2 (30 wt %) were added, followed by adding an ice-cold, fresh prepared aqueous solution of sodium borohydride (0.1 M 1.2 mL) with vigorous stirring. After 5 min of stirring, the solution was left undisturbed for 2 h. The synthesized Ag nanoseeds were concentrated by centrifugation and washed with water twice before

use. Second, 50 nm Au nanoplates were prepared as follows: To 44 mL of water, 300 μ L of ascorbic acid (0.1 M), 200 μ L sodium citrate (0.075 M), and Ag seeds were added, followed by adding 240 μ L of silver nitrate (0.1 M) with vigorous stirring for 30 min. The Ag nanoplates were centrifuged and washed with water for future use. Ag nanoplates of different sizes were obtained by changing the amount of Ag seeds added.

Preparation of Au Nanorings. Au nanorings were prepared according to previous literature with some modifications.⁵⁰ First, Ag@Au nanoplates were prepared as follows: Basic hydroxylamine hydrochloride solution (3 mM) was prepared according to a previous report.⁵⁰ The as-prepared Ag nanoplates were dissolved in 20 mL of water in a glass container placed in an ice bath. To this solution, the basic hydroxylamine hydrochloride and an aqueous solution of hydrogen tetrachloroaurate(III) trihydrate ($\text{HAuCl}_4 \cdot 3\text{H}_2\text{O}$, 0.3 mM) were added *via* syringe pump at a rate of 2 mL/h with vigorous stirring. The reaction was monitored by UV–vis spectroscopy to determine the end of pumping. The Ag@Au nanoplates were centrifuged and washed with water. Second, the thin Au nanorings were prepared as follows: The as-prepared Ag nanoplates were incubated with 5 mL solution of bis(*p*-sulfonatophenyl)-phenylphosphine dihydrate dipotassium (2 mM) to etch the Ag templates. The reaction was monitored by UV–vis spectroscopy to indicate the completion of etching. The resulting thin Au nanorings were centrifuged and washed with water for three times before use. Finally, to prepare Au nanorings with different thicknesses, the thin Au nanorings were dispersed in 20 mL of water. The above basic hydroxylamine hydrochloride solution and aqueous solution of $\text{HAuCl}_4 \cdot 3\text{H}_2\text{O}$ were added *via* syringe pump at a rate of 2 mL/h with vigorous stirring. The reaction was monitored by UV–vis spectroscopy to determine the thickness of Au nanorings.

Preparation of Au Nanoplates. Au nanoplates were prepared according to previous literature with some modifications.⁵¹ The as-prepared Ag nanoplates were dispersed in 20 mL of water in a glass container placed in an ice bath. The basic hydroxylamine hydrochloride and the aqueous solution of hydrogen tetrachloroaurate (III) trihydrate (0.3 mM) were added *via* syringe pump at a rate of 2 mL/h with vigorous stirring. Along with pumping, the main absorption peak of the solution was first red-shifted and then blue-shifted. The reaction was stopped when the major absorption peak was around 680 nm. The Au nanoplates were centrifuged and washed with water for 2 times before use.

Preparation of Au Nanospheres. Au nanospheres of 50 nm were prepared by a previously reported method.⁵²

PEGylation of AuNPs. A 50 μ L of concentrated aqueous solution of AuNPs was added to 1 mL of water with excess of HS-PEG. The mixed solutions were placed in a shaker for 24 h. All AuNPs were centrifuged and washed with water for 3 times to remove the free HS-PEG.

ASSOCIATED CONTENT

Supporting Information

The Supporting Information is available free of charge on the ACS Publications website at DOI: 10.1021/acsnano.7b05908.

Experimental details (PDF)

AUTHOR INFORMATION

Corresponding Authors

*E-mail: shawn.chen@nih.gov.

*E-mail: znie@umd.edu.

ORCID

Jibin Song: 0000-0003-4771-5006

Zhihong Nie: 0000-0001-9639-905X

Xiaoyuan Chen: 0000-0002-9622-0870

Author Contributions

[∇]These authors contributed equally.

Notes

The authors declare no competing financial interest.

ACKNOWLEDGMENTS

The work was supported by the Intramural Research Program of the National Institute of Biomedical Imaging and Bioengineering, National Institutes of Health. We acknowledge Maryland NanoCenter and its NispLab. NispLab is supported, in part, by the NSF in partnership with MRSEC Shared Experimental Facilities.

REFERENCES

- (1) Albanese, A.; Tang, P. S.; Chan, W. C. W. The Effect of Nanoparticle Size, Shape, and Surface Chemistry on Biological Systems. *Annu. Rev. Biomed. Eng.* **2012**, *14*, 1–16.
- (2) Toy, R.; Peiris, P. M.; Ghaghada, K. B.; Karathanasis, E. Shaping Cancer Nanomedicine: The Effect of Particle Shape on the *In Vivo* Journey of Nanoparticles. *Nanomedicine* **2014**, *9*, 121–134.
- (3) Tang, L.; Yang, X.; Yin, Q.; Cai, K.; Wang, H.; Chaudhury, I.; Yao, C.; Zhou, Q.; Kwon, M.; Hartman, J. A.; Dobrucki, I. T.; Dobrucki, L. W.; Borst, L. B.; Lezmi, S.; Helferich, W. G.; Ferguson, A. L.; Fan, T. M.; Cheng, J. Investigating the Optimal Size of Anticancer Nanomedicine. *Proc. Natl. Acad. Sci. U. S. A.* **2014**, *111*, 15344–15349.
- (4) Matsumoto, Y.; Nichols, J. W.; Toh, K.; Nomoto, T.; Cabral, H.; Miura, Y.; Christie, R. J.; Yamada, N.; Ogura, T.; Kano, M. R.; Matsumura, Y.; Nishiyama, N.; Yamasoba, T.; Bae, Y. H.; Kataoka, K. Vascular Bursts Enhance Permeability of Tumour Blood Vessels and Improve Nanoparticle Delivery. *Nat. Nanotechnol.* **2016**, *11*, 533–538.
- (5) Matsumura, Y.; Maeda, H. A New Concept for Macromolecular Therapeutics in Cancer Chemotherapy: Mechanism of Tumor-tropic Accumulation of Proteins and the Antitumor Agent SMANCS. *Cancer Res.* **1986**, *46*, 6387–6382.
- (6) Setyawati, M. I.; Tay, C. Y.; Chia, S. L.; Goh, S. L.; Fang, W.; Neo, M. J.; Chong, H. C.; Tan, S. M.; Loo, S. C. J.; Ng, K. W.; Xie, J. P.; Ong, C. N.; Tan, N. S.; Leong, D. T. Titanium Dioxide Nanomaterials Cause Endothelial Cell Leakiness by Disrupting the Homophilic Interaction of VE-Cadherin. *Nat. Commun.* **2013**, *4*, 1673.
- (7) Setyawati, M. I.; Tay, C. Y.; Docter, D.; Stauber, R. H.; Leong, D. T. Understanding and Exploiting Nanoparticles' Intimacy with the Blood Vessel and Blood. *Chem. Soc. Rev.* **2015**, *44*, 8174–8199.

- (8) Elsabahy, M.; Wooley, K. L. Design of Polymeric Nanoparticles for Biomedical Delivery Applications. *Chem. Soc. Rev.* **2012**, *41*, 2545–2561.

- (9) Blanco, E.; Shen, H.; Ferrari, M. Principles of Nanoparticle Design for Overcoming Biological Barriers to Drug Delivery. *Nat. Biotechnol.* **2015**, *33*, 941–951.

- (10) Tsoi, K. M.; MacParland, S. A.; Ma, X.-Z.; Spetzler, V. N.; Echeverri, J.; Ouyang, B.; Fadel, S. M.; Sykes, E. A.; Goldaracena, N.; Kathis, J. M.; Conneely, J. B.; Alman, B. A.; Selzner, M.; Ostrowski, M. A.; Adeyi, O. A.; Zilman, A.; McGilvray, I. D.; Chan, W. C. W. Mechanism of Hard-Nanomaterial Clearance by the Liver. *Nat. Mater.* **2016**, *15*, 1212–1221.

- (11) Nel, A. E.; Madler, L.; Velegol, D.; Xia, T.; Hoek, E. M. V.; Somasundaran, P.; Klaessig, F.; Castranova, V.; Thompson, M. Understanding Biophysicochemical Interactions at the Nano-Bio Interface. *Nat. Mater.* **2009**, *8*, 543–557.

- (12) Cheng, L.-C.; Jiang, X.; Wang, J.; Chen, C.; Liu, R.-S. Nano-Bio Effects: Interaction of Nanomaterials with Cells. *Nanoscale* **2013**, *5*, 3547–3569.

- (13) Pelaz, B.; del Pino, P.; Maffre, P.; Hartmann, R.; Gallego, M.; Rivera-Fernández, S.; de la Fuente, J. M.; Nienhaus, G. U.; Parak, W. J. Surface Functionalization of Nanoparticles with Polyethylene Glycol: Effects on Protein Adsorption and Cellular Uptake. *ACS Nano* **2015**, *9*, 6996–7008.

- (14) Huang, X.; El-Sayed, I. H.; Qian, W.; El-Sayed, M. A. Cancer Cell Imaging and Photothermal Therapy in the Near-Infrared Region by Using Gold Nanorods. *J. Am. Chem. Soc.* **2006**, *128*, 2115–2120.

- (15) Dreaden, E. C.; Alkilany, A. M.; Huang, X.; Murphy, C. J.; El-Sayed, M. A. The Golden Age: Gold Nanoparticles for Biomedicine. *Chem. Soc. Rev.* **2012**, *41*, 2740–2779.

- (16) Abadeer, N. S.; Murphy, C. J. Recent Progress in Cancer Thermal Therapy Using Gold Nanoparticles. *J. Phys. Chem. C* **2016**, *120*, 4691–4716.

- (17) Liu, Y.; He, J.; Yang, K.; Yi, C.; Liu, Y.; Nie, L.; Khashab, N. M.; Chen, X.; Nie, Z. Folding Up of Gold Nanoparticle Strings into Plasmonic Vesicles for Enhanced Photoacoustic Imaging. *Angew. Chem., Int. Ed.* **2015**, *54*, 15809–15812.

- (18) Black, K. C. L.; Wang, Y.; Luehmann, H. P.; Cai, X.; Xing, W.; Pang, B.; Zhao, Y.; Cutler, C. S.; Wang, L. V.; Liu, Y.; Xia, Y. Radioactive ¹⁹⁸Au-Doped Nanostructures with Different Shapes for *In Vivo* Analyses of Their Biodistribution, Tumor Uptake, and Intratumoral Distribution. *ACS Nano* **2014**, *8*, 4385–4394.

- (19) Deng, H.; Zhong, Y. Q.; Du, M. H.; Liu, Q. J.; Fan, Z. M.; Dai, F. Y.; Zhang, X. Theranostic Self-Assembly Structure of Gold Nanoparticles for NIR Photothermal Therapy and X-Ray Computed Tomography Imaging. *Theranostics* **2014**, *4*, 904–918.

- (20) Yang, Z.; Song, J.; Dai, Y.; Chen, J.; Wang, F.; Lin, L.; Liu, Y.; Zhang, F.; Yu, G.; Zhou, Z.; Fan, W.; Huang, W.; Fan, Q.; Chen, X. Self-Assembly of Semiconducting-Plasmonic Gold Nanoparticles with Enhanced Optical Property for Photoacoustic Imaging and Photothermal Therapy. *Theranostics* **2017**, *7*, 2177–2185.

- (21) Cabral, H.; Matsumoto, Y.; Mizuno, K.; Chen, Q.; Murakami, M.; Kimura, M.; Terada, Y.; Kano, M. R.; Miyazono, K.; Uesaka, M.; Nishiyama, N.; Kataoka, K. Accumulation of Sub-100 nm Polymeric Micelles in Poorly Permeable Tumours Depends on Size. *Nat. Nanotechnol.* **2011**, *6*, 815–823.

- (22) Petros, R. A.; DeSimone, J. M. Strategies in the Design of Nanoparticles for Therapeutic Applications. *Nat. Rev. Drug Discovery* **2010**, *9*, 615–627.

- (23) Arnida; Janát-Amsbury, M. M.; Ray, A.; Peterson, C. M.; Ghandehari, H. Geometry and Surface Characteristics of Gold Nanoparticles Influence Their Biodistribution and Uptake by Macrophages. *Eur. J. Pharm. Biopharm.* **2011**, *77*, 417–423.

- (24) Song, J.; Yang, X.; Yang, Z.; Lin, L.; Liu, Y.; Zhou, Z.; Shen, Z.; Yu, G.; Dai, Y.; Jacobson, O.; Munasinghe, J.; Yung, B.; Teng, G.-J.; Chen, X. Rational Design of Branched Nanoporous Gold Nanoshells with Enhanced Physico-Optical Properties for Optical Imaging and Cancer Therapy. *ACS Nano* **2017**, *11*, 6102–6113.

- (25) Yavuz, M. S.; Cheng, Y.; Chen, J.; Cobley, C. M.; Zhang, Q.; Rycenga, M.; Xie, J.; Kim, C.; Song, K. H.; Schwartz, A. G.; Wang, L. V.; Xia, Y. Gold Nanocages Covered by Smart Polymers for Controlled Release with Near-Infrared Light. *Nat. Mater.* **2009**, *8*, 935–939.
- (26) Kolhar, P.; Anselmo, A. C.; Gupta, V.; Pant, K.; Prabhakarandian, B.; Ruoslahti, E.; Mitragotri, S. Using Shape Effects to Target Antibody-Coated Nanoparticles to Lung and Brain Endothelium. *Proc. Natl. Acad. Sci. U. S. A.* **2013**, *110*, 10753–10758.
- (27) Peiris, P. M.; Toy, R.; Doolittle, E.; Pansky, J.; Abramowski, A.; Tam, M.; Vicente, P.; Tran, E.; Hayden, E.; Camann, A.; Mayer, A.; Erokwu, B. O.; Berman, Z.; Wilson, D.; Baskaran, H.; Flask, C. A.; Kerl, R. A.; Karathanasis, E. Imaging Metastasis Using an Integrin-Targeting Chain-Shaped Nanoparticle. *ACS Nano* **2012**, *6*, 8783–8795.
- (28) Anselmo, A. C.; Modery-Pawlowski, C. L.; Menegatti, S.; Kumar, S.; Vogus, D. R.; Tian, L. L.; Chen, M.; Squires, T. M.; Sen Gupta, A.; Mitragotri, S. Platelet-Like Nanoparticles: Mimicking Shape, Flexibility, and Surface Biology of Platelets to Target Vascular Injuries. *ACS Nano* **2014**, *8*, 11243–11253.
- (29) Herd, H.; Daum, N.; Jones, A. T.; Huwer, H.; Ghandehari, H.; Lehr, C.-M. Nanoparticle Geometry and Surface Orientation Influence Mode of Cellular Uptake. *ACS Nano* **2013**, *7*, 1961–1973.
- (30) Zhang, Y.; Tekobo, S.; Tu, Y.; Zhou, Q.; Jin, X.; Dergunov, S. A.; Pinkhassik, E.; Yan, B. Permission to Enter Cell by Shape: Nanodisk vs. Nanosphere. *ACS Appl. Mater. Interfaces* **2012**, *4*, 4099–4105.
- (31) Chen, M.; Tang, S.; Guo, Z.; Wang, X.; Mo, S.; Huang, X.; Liu, G.; Zheng, N. Core–Shell Pd@Au Nanoplates as Theranostic Agents for *In Vivo* Photoacoustic Imaging, CT Imaging, and Photothermal Therapy. *Adv. Mater.* **2014**, *26*, 8210–8216.
- (32) Hu, Y.; Yang, Y.; Wang, H.; Du, H. Synergistic Integration of Layer-by-Layer Assembly of Photosensitizer and Gold Nanorings for Enhanced Photodynamic Therapy in the Near Infrared. *ACS Nano* **2015**, *9*, 8744–8754.
- (33) Song, J.; Wang, F.; Yang, X.; Ning, B.; Harp, M. G.; Culp, S. H.; Hu, S.; Huang, P.; Nie, L.; Chen, J.; Chen, X. Gold Nanoparticle Coated Carbon Nanotube Ring with Enhanced Raman Scattering and Photothermal Conversion Property for Theranostic Applications. *J. Am. Chem. Soc.* **2016**, *138*, 7005–7015.
- (34) Champion, J. A.; Mitragotri, S. Role of Target Geometry in Phagocytosis. *Proc. Natl. Acad. Sci. U. S. A.* **2006**, *103*, 4930–4934.
- (35) Shi, X.; von dem Bussche, A.; Hurt, R. H.; Kane, A. B.; Gao, H. Cell Entry of One-Dimensional Nanomaterials Occurs by Tip Recognition and Rotation. *Nat. Nanotechnol.* **2011**, *6*, 714–719.
- (36) Aizpurua, J.; Hanarp, P.; Sutherland, D. S.; Käll, M.; Bryant, G. W.; García de Abajo, F. J. Optical Properties of Gold Nanorings. *Phys. Rev. Lett.* **2003**, *90*, 057401.
- (37) Chen, H.; Shao, L.; Ming, T.; Sun, Z.; Zhao, C.; Yang, B.; Wang, J. Understanding the Photothermal Conversion Efficiency of Gold Nanocrystals. *Small* **2010**, *6*, 2272–2280.
- (38) Sykes, E. A.; Chen, J.; Zheng, G.; Chan, W. C. W. Investigating the Impact of Nanoparticle Size on Active and Passive Tumor Targeting Efficiency. *ACS Nano* **2014**, *8*, 5696–5706.
- (39) Barua, S.; Yoo, J.-W.; Kolhar, P.; Wakankar, A.; Gokarn, Y. R.; Mitragotri, S. Particle Shape Enhances Specificity of Antibody-Displaying Nanoparticles. *Proc. Natl. Acad. Sci. U. S. A.* **2013**, *110*, 3270–3275.
- (40) Gao, H.; Shi, W.; Freund, L. B. Mechanics of Receptor-Mediated Endocytosis. *Proc. Natl. Acad. Sci. U. S. A.* **2005**, *102*, 9469–9474.
- (41) Nambara, K.; Niikura, K.; Mitomo, H.; Ninomiya, T.; Takeuchi, C.; Wei, J.; Matsuo, Y.; Ijro, K. Reverse Size Dependences of the Cellular Uptake of Triangular and Spherical Gold Nanoparticles. *Langmuir* **2016**, *32*, 12559–12567.
- (42) Lesniak, A.; Salvati, A.; Santos-Martinez, M. J.; Radomski, M. W.; Dawson, K. A.; Åberg, C. Nanoparticle Adhesion to the Cell Membrane and Its Effect on Nanoparticle Uptake Efficiency. *J. Am. Chem. Soc.* **2013**, *135*, 1438–1444.
- (43) Chithrani, B. D.; Chan, W. C. W. Elucidating the Mechanism of Cellular Uptake and Removal of Protein-Coated Gold Nanoparticles of Different Sizes and Shapes. *Nano Lett.* **2007**, *7*, 1542–1550.
- (44) Sun, X.; Huang, X.; Yan, X.; Wang, Y.; Guo, J.; Jacobson, O.; Liu, D.; Szajek, L. P.; Zhu, W.; Niu, G.; Kiesewetter, D. O.; Sun, S.; Chen, X. Chelator-Free ⁶⁴Cu-Integrated Gold Nanomaterials for Positron Emission Tomography Imaging Guided Photothermal Cancer Therapy. *ACS Nano* **2014**, *8*, 8438–8446.
- (45) Roger, R. P.; Hussey, R. G. Stokes Drag on a Flat Annular Ring. *Phys. Fluids* **1982**, *25*, 915–922.
- (46) Zhang, B.; Lan, T.; Huang, X.; Dong, C.; Ren, J. Sensitive Single Particle Method for Characterizing Rapid Rotational and Translational Diffusion and Aspect Ratio of Anisotropic Nanoparticles and Its Application in Immunoassays. *Anal. Chem.* **2013**, *85*, 9433–9438.
- (47) Tay, C. Y.; Setyawati, M. I.; Leong, D. T. Nanoparticle Density: A Critical Biophysical Regulator of Endothelial Permeability. *ACS Nano* **2017**, *11*, 2764–2772.
- (48) Setyawati, M. I.; Mochalin, V. N.; Leong, D. T. Tuning Endothelial Permeability with Functionalized Nanodiamonds. *ACS Nano* **2016**, *10*, 1170–1181.
- (49) Zhang, Q.; Li, N.; Goebel, J.; Lu, Z.; Yin, Y. A Systematic Study of the Synthesis of Silver Nanoplates: Is Citrate a “Magic” Reagent? *J. Am. Chem. Soc.* **2011**, *133*, 18931–18939.
- (50) Shahjamali, M. M.; Bosman, M.; Cao, S.; Huang, X.; Cao, X.; Zhang, H.; Pramana, S. S.; Xue, C. Surfactant-Free Sub-2 nm Ultrathin Triangular Gold Nanoframes. *Small* **2013**, *9*, 2880–2886.
- (51) Shahjamali, M. M.; Bosman, M.; Cao, S.; Huang, X.; Saadat, S.; Martinsson, E.; Aili, D.; Tay, Y. Y.; Liedberg, B.; Loo, S. C. J.; Zhang, H.; Boey, F.; Xue, C. Gold Coating of Silver Nanoprisms. *Adv. Funct. Mater.* **2012**, *22*, 849–854.
- (52) Liu, Y.; Yang, X.; Huang, Z.; Huang, P.; Zhang, Y.; Deng, L.; Wang, Z.; Zhou, Z.; Liu, Y.; Kalish, H.; Khachab, N. M.; Chen, X.; Nie, Z. Magneto-Plasmonic Janus Vesicles for Magnetic Field-Enhanced Photoacoustic and Magnetic Resonance Imaging of Tumors. *Angew. Chem.* **2016**, *128*, 15523–15526.